

The dynamic response and seismic damage of single-layer reticulated shells subjected to near-fault ground motions

Ming Zhang^{*1}, Gerry Parke² and Zhiwang Chang¹

¹School of Civil Engineering, Southwest Jiaotong University, Chengdu 610031, China

²Department of Civil and Environmental Engineering, University of Surrey, Guildford GU2 7XH, UK

(Received February 9, 2018, Revised February 28, 2018, Accepted March 3, 2018)

Abstract. The dynamic response and seismic damage of single-layer reticulated shells in the near field of a rupturing fault can be different from those in the far field due to the different characteristics in the ground motions. To investigate the effect, the dynamic response and seismic damage of this spatial structures subjected to two different ground motions were numerically studied by nonlinear dynamic response analysis. Firstly, twelve seismic waves with an apparent velocity pulse, including horizontal and vertical seismic waves, were selected to represent the near-fault ground motion characteristics. In contrast, twelve seismic records recorded at the same site from other or same events where the epicenter was far away from the site were employed as the far-fault ground motions. Secondly, the parametric modeling process of Kiewitt single-layer reticulated domes using the finite-element package ANSYS was described carefully. Thirdly, a nonlinear time-history response analysis was carried out for typical domes subjected to different earthquakes, followed by analyzing the dynamic response and seismic damage of this spatial structures under two different ground motions based on the maximum nodal displacements and Park-Ang index as well as dissipated energy. The results showed that this spatial structures in the near field of a rupturing fault exhibit a larger dynamic response and seismic damage than those obtained from far-fault ground motions. In addition, the results also showed that the frequency overlap between structures and ground motions has a significant influence on the dynamic response of the single-layer reticulated shells, the duration of the ground motions has little effects.

Keywords: single-layer reticulated shells; near-fault ground motions; far-fault ground motions; nonlinear dynamic analysis; frequencies; duration

1. Introduction

Since the first single-pulse shock recording of the Port Hueneme accelerogram of March 18, 1957, engineers started to pay attention to the corresponding earthquake-resistant construction (Housner 1958). Research over the last decade has shown that pulse-type earthquake ground motions that result from forward-directivity effects can result in significant damage to structures (Rodriguez-Marek and Cofer 2007). And analytical models indicated that traditional analysis methods were insufficient to capture the full effects of pulse-type ground motions due to lack of near-fault records. Fortunately, the recent increase in the number of recorded ground motions has allowed a better understanding of the hazardous effects of the pulse-type ground motions on structures. Hence, the structural responses under the near-fault ground motions have been investigated from various viewpoints and some conclusions can be obtained from these references (Kotaro and Izuru 2015).

Firstly, the near-fault ground motions have the potential to cause more severe damage to the base-isolated buildings (Kaoru *et al.* 2011, Fabio and Mirko 2016), steel structural

buildings (Minasidis *et al.* 2014, Enderami *et al.* 2014), long-span structures (Zhang and Wang 2013, Wu *et al.* 2014, Yang *et al.* 2017), and high-rise flexible structures (Hall *et al.* 1995, Masaeli *et al.* 2014) than far-fault ground motions. Secondly, the near-fault ground motions are seen to possess large energy close to the structure's initial natural frequency and the elastic-plastic structure is easier to be damaged than others (Kaoru *et al.* 2011, Wu *et al.* 2014, Mavroeidis *et al.* 2004, Ueno *et al.* 2010, Alonso-Rodriguez and Miranda 2015, Cao *et al.* 2016), namely, the seismic responses increase with the pulse period of near-fault ground motions. Thirdly, the structural inelastic seismic response has an obviously increasing value under the action of near-fault ground motions (Kotaro and Izuru 2015, Mavroeidise *et al.* 2004, Ueno *et al.* 2010, Kalkan and Kunnath 2006). In some situations, the existing design methods, such as square root of the sum of the squares (SRSS) and complete quadratic combination (CQC), will underestimate the inelastic displacement of the structures subjected to the critical earthquake load (Yang *et al.* 2017). Fourth, the existing seismic design codes for buildings either improve the seismic design force requirements of the structures (IBC-2012 2011, CPA 2011) or forbid the building of important structures in hazardous areas including the near-fault source (GB 50011-2010 2010). This is because further improvement in the design of a sound structure in hazardous areas is required.

Also it can be found from these references that the

*Corresponding author, Ph.D.

E-mail: zhangming@home.swjtu.edu.cn

Table 1 Description of near-fault and far-fault seismic waves used in this paper (Wang *et al.* 2014)

No.	Ground motion	Earthquake	Distance to fault (km)	Station location	M_w	Comp.	PGA (cm/s ²)	PGV (cm/s)	PGV/PGA (s)
1	Near-fault	Northridge 1994	7.1	Newhall, CA-Los Angeles County Fire #24279	6.7	360	578.20	94.70	0.164
2	Far-fault	Northridge 1994	18.4	Los Angeles, CA-Fire Station 108 #5314	6.7	35	576.90	29.39	0.051
3	Near-fault	Northridge 1994	8.6	Sylmar, CA-Jensen Filtration Plant #655	6.7	22	560.30	77.23	0.138
4	Far-fault	Northridge 1994	29.4	Warm Springs #24272	6.7	90	221.20	13.35	0.060
5	Near-fault	Northridge 1994	8.6	Los Angeles Reservoir #2141	6.7	64	317.60	47.61	0.149
6	Far-fault	Northridge 1994	17.9	Tarzana, CA-Cedar Hill #24436	5.3	90	365.30	11.78	0.032
7	Near-fault	Imperial Valley 1979	5.2	El Centro, CA-Array Sta 5 #0952	6.5	230	360.37	95.89	0.266
8	Far-fault	Imperial Valley 1979	21.7	El Centro, CA-Array Sta 13 #5059	6.5	230	131.10	11.89	0.091
9	Near-fault	Imperial Valley 1979	8.8	Holtville, CA-Post Office #5055	6.5	225	243.00	51.90	0.214
10	Far-fault	Imperial Valley 1979	21.8	Superstition Mtn, CA-Camera Site #0286	6.5	135	182.20	8.65	0.048
11	Near-fault	Loma Prieta 1989	6.3	Gilroy Array Sta 3 # 47381	6.5	90	362.00	43.80	0.121
12	Far-fault	Loma Prieta 1989	15.6	Gilroy Array Sta 7 # 57425	6.5	90	314.30	16.30	0.052
13	Near-fault	Loma Prieta 1989	2.8	Corralitos, CA #57007	6.5	90	469.40	47.50	0.101
14	Far-fault	Loma Prieta 1989	16.9	Coyote Lake Dam, CA #57217	6.5	285	471.00	37.50	0.079
15	Near-fault	Chi-Chi 1999	8.9	Taichung, Taiwan #TCU050	7.6	90	142.70	32.40	0.227
16	Far-fault	Chi-Chi 1999	32.0	Ilan, Taiwan #ILA067	7.6	90	195.70	11.40	0.058
17	Near-fault	Chi-Chi 1999	7.9	Taichung, Taiwan #TCU072	7.6	90	466.90	70.80	0.152
18	Far-fault	Tohoku Japan 2011	131.0	KNET station MYG004	9.0	N-S	2699.89	106.16	0.039
19	Near-fault	Chi-Chi 1999	3.2	Taichung, Taiwan #TCU076	7.6	90	336.10	59.00	0.176
20	Far-fault	El Salvador 2001	96.0	UCA station LI	7.6	0	1154.60	56.67	0.049
21	Near-fault	Chi-Chi 1999	3.4	CWB station TCU075	7.6	Up	223.80	51.10	0.228
22	Far-fault	Chi-Chi 1999	13.2	CWB station TCU088	7.6	Up	223.70	12.70	0.057
23	Near-fault	Chi-Chi 1999	5.6	CWB station TCU055	7.6	Up	152.30	58.50	0.384
24	Far-fault	Chi-Chi 1999	24.7	CWB station TCU045	7.6	Up	331.80	18.90	0.057

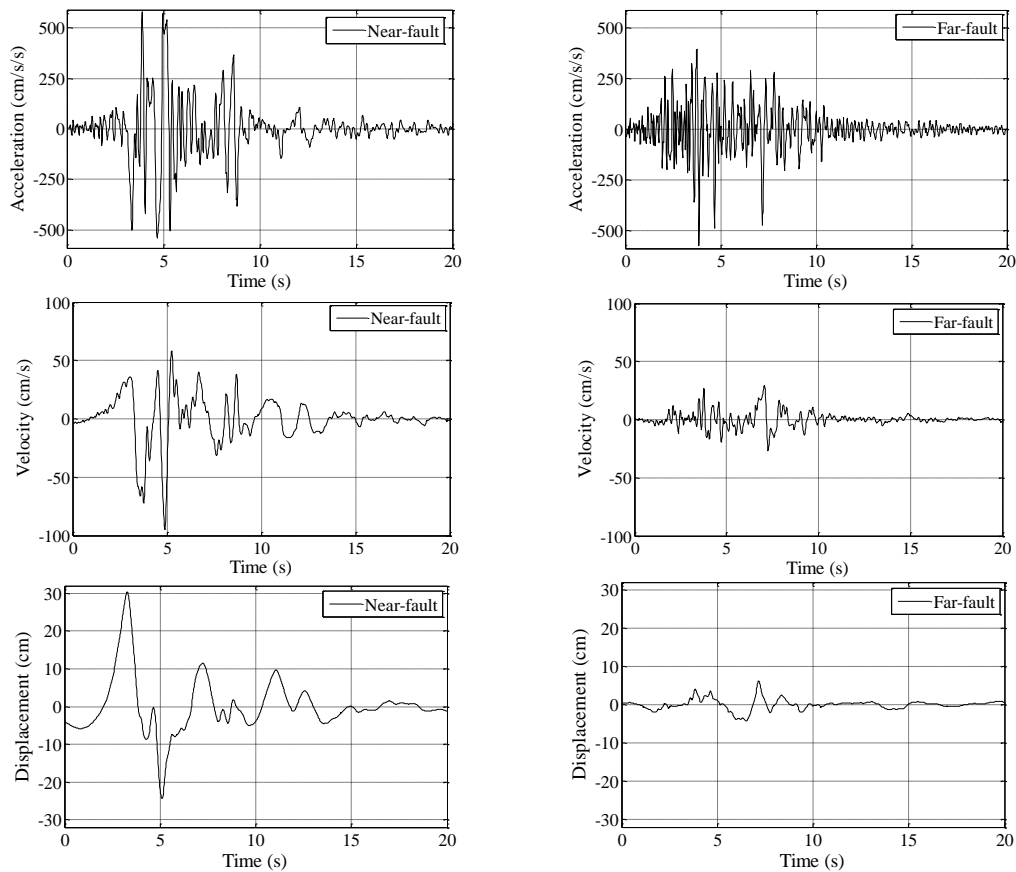
seismic response of a single-layer reticulated shell subjected to near-fault ground motions has not been investigated up to the present, but which has been widely used in spatial structures in recent decades (Yu *et al.* 2011, Bai *et al.* 2015) because of their strong aesthetic appearance, ability to cover large spaces and sound structural performance. Meanwhile, current research on single-layer reticulated shell is mainly focused on structural response (Liu and Li 2010, Zhai *et al.* 2013, Zhai and Wang 2013, Nie *et al.* 2014, Kong *et al.* 2014, Li, *et al.* 2014, Fan *et al.* 2014, Ma *et al.* 2014), collapse (Ye *et al.* 2011, Ye *et al.* 2011, Liu and Ye 2014, Ma *et al.* 2015, Zhong *et al.* 2016) of the space steel structures under far-fault ground motions through experiment and numerical simulation analysis (Ma *et al.* 2013, Zhu and Ye 2014, Yan *et al.* 2014, Ma *et al.* 2015, Ba *et al.* 2015), in addition to stability and buckling (Fan *et al.* 2010, Ramalingam and Jayachandran 2015, Bruno *et al.* 2016, Yan *et al.* 2016).

In view of the above analyses, the nonlinear time-history response analysis was carried out with the finite-element

package ANSYS for typical single-layer reticulated shells subjected to different near-fault and far-fault ground motions in order to investigate the structural response to near-source ground motions. Then the comparison of the seismic responses for single-layer reticulated shells was conducted investigating the deformation and strain energy. Based on the displacement and the structural dissipated energy, the seismic structural damage level of typical shells subjected to near-fault and far-fault ground motions are assessed based on the structural damage index D_s (Park and Ang 1985, Du *et al.* 2007), and some seismic resistance measures for single-layer reticulated shells built near the near-fault regions are provided. Lastly, the effects that the frequencies of the ground motions and the single-layer shell have on the seismic response is discussed.

2. Near-fault and far-fault seismic waves

As mentioned in reference (Malhotra 1999), ground



(a) Near-fault seismic wave from Newhall station

(b) Far-fault seismic wave from Los Angeles station

Fig. 1 The time histories of seismic waves in Northridge earthquake including acceleration, velocity and displacement (Zhang and Wang 2013)

motions affected by directivity focusing at near-field stations contain distinct pulses in the acceleration, velocity, and displacement histories. And the effect of directivity focusing is most pronounced on displacements, less on velocities, and least on accelerations. Hence, the impulsive character occurring over long periods, in the velocity and displacement histories, is one of the key characteristics of the near-fault seismic waves (Zhang and Wang 2013), which may induce a dramatically high response in long period structures. Based on the impulsive characteristic of the near-fault seismic waves, twelve seismic waves with an apparent velocity pulse, including horizontal and vertical seismic waves, were selected to represent the near-fault ground motion characteristics. In contrast, twelve seismic records recorded at the same site from other or same events where the epicenter was far away from the site were employed as the far-fault ground motions. These seismic waves came from the 1994 Northridge, 1979 Imperial Valley, 1989 Loma Prieta, 1999 Chi-Chi, 2011 Tohoku Japan and 2001 El Salvador earthquakes referring to reference (Zhang and Wang 2013). For further details, Table 1 depicts the properties of the records obtained from the database of COSMOS (COSMOS Virtual Data Center). Compared to far-fault records, all of the selected near-fault records display ground motions with an apparent velocity pulse whose pulse duration is very close to or greater than 1.0 s, and have a high PGV/PGA ratio which is larger than 0.1s. The comparison between the

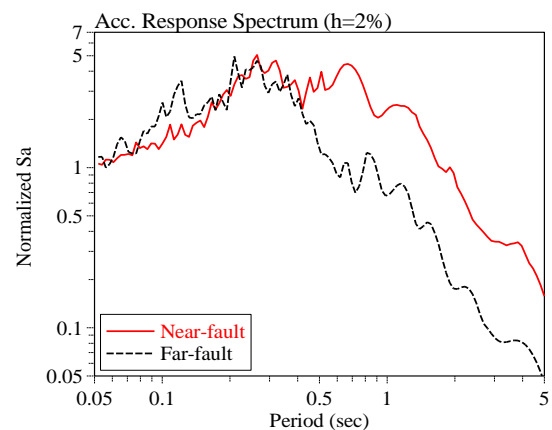


Fig. 2 Acceleration spectrum of near-fault and far fault seismic waves corresponding to Fig. 1

near-fault and far-fault seismic waves, including the acceleration, velocity and displacement time histories, are shown in Fig. 1 as an example. Meanwhile, Fig. 2 presents the Normalized acceleration-Period spectrum with a damping ratio of 2% corresponding to seismic waves in Fig. 1.

It can be seen from Fig. 1 that there are distinct differences in the amplitude between the near-fault and far-fault records for the velocity and displacement pulse. For the acceleration, the long period seismic response of the near-fault seismic wave takes up a larger part of the

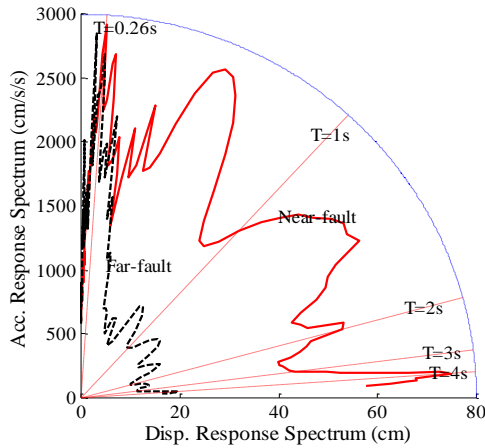


Fig. 3 Acceleration-deformation spectrum of near-fault and far-fault ground motions corresponding to Fig. 2

acceleration response spectrum compared to that in far-fault seismic acceleration response spectrum.

Refer to the acceleration-deformation response spectrum (Malhotra 1999), Fig. 3 presents the relationship of the acceleration response spectrum against the displacement response spectrum of near-fault and far-fault ground motions corresponding to Fig. 2. The natural period T in this figure is indicated by radial dotted lines passing through the origin. It can be seen from Fig. 3 that the responses, including acceleration and displacement responses, of the near-fault ground motion are more excessive than that of the far-fault ground motion, starting from the natural period $T=0.26$ s. After $T=0.26$ s, the gap becomes greater between the near-fault and far-fault ground motions, which makes us contemplating the seismic influences of the near-fault ground motions on the single-layer reticulated shells whose natural periods are larger than 0.26s.

In the analyses all of the seismic waves were regularized to have the peak ground acceleration (PGA) equal to 1 g, and the 90% energy duration T_d ($T_d=T_2-T_1$, $\Delta E=E(T_2)-E(T_1)=90\%E_a$, E_a is the total energy) (Brandes and Vogel 1998) is adopted to determine the duration of the seismic waves. The reason for selecting large an amplitude (PGA equals 1 g) is the fact that the near-fault ground motions are exceptionally strong, such as the large PGA 2.69 g recorded by KNET station MYG004 in the Tohoku Japan earthquake shown in Table 1, and it is very likely that the single-layer reticulated shells will undergo these extremely large seismic waves as they sometimes lie in the near-fault regions.

3. Dome models

The structural model and the classification for Kiewitt single-layer reticulated domes (Zhi *et al.* 2007) are shown in Figs. 4 and 5. The chosen spans (L) are 40m, 50m and 60m and the rise to span ratios (f/L) are 1/3, 1/5 and 1/7 respectively. These domes were subjected to different near-fault ground motions and were analyzed in the following sections. Single-layer reticulated domes were designed in the normal way (the tube cross-sections are shown in Table

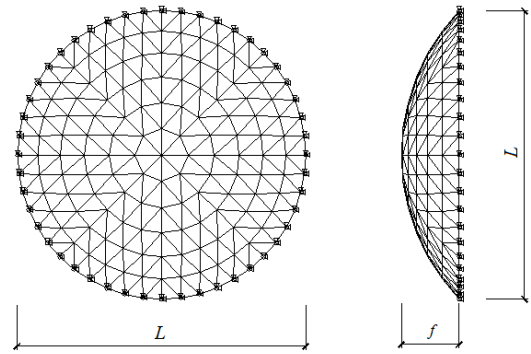


Fig. 4 Single-layer reticulated dome of Kiewitt system

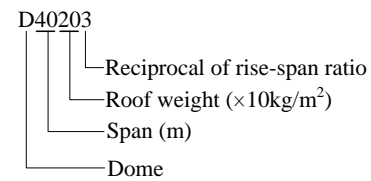


Fig. 5 Classification of single-layer reticulated domes (Zhi *et al.* 2007)

Table 2 Labels and parameters of the shell models

Shell label	Span (m)	Roof weight including cladding (kg/m^2)	Rise to span ratio	Cross section (mm)	
				radial and hoop members	oblique members
D40203	40	200	1/3	146×5	140×6
D40205	40	200	1/5	146×5	140×6
D40207	40	200	1/7	146×5	140×6
D50063	50	60	1/3	168×6	152×5
D50065	50	60	1/5	168×6	152×5
D50067	50	60	1/7	168×6	152×5
D60063	60	60	1/3	194×6	168×6
D60065	60	60	1/5	194×6	168×6
D60067	60	60	1/7	194×6	168×6

2). All the supports for the domes fixed against translation but free for rotation. Geometrical and material nonlinearity were considered in the dynamic analysis, and the bilinear kinematic hardening elastic-plastic model in the ANSYS database (ANSYS 10.0 2005) was adopted. Here, the model had a yield stress of 235 MPa, Young's modulus E_1 (initial slope) of 206 GPa and Young's modulus E_2 (the second slope) of $0.02E_1$. The Rayleigh damping was composed of the first and second natural vibration frequencies and the damping ratio was empirically set at 0.02. The PIPE20 element (ANSYS 10.0 2005) in the element library of ANSYS was selected to simulate the dome members. Nonlinear time-history response was simulated using the finite-element package ANSYS.

The nonlinear dynamic time history analysis, including geometric nonlinearity and material nonlinearity, was adopted for investigating the seismic response of the single-layer reticulated shell subjected to near-fault and far-fault ground motions. As a result, the representative responses, such as frequencies, the ultimate elastic displacement, maximum displacement, dissipated energy increment and

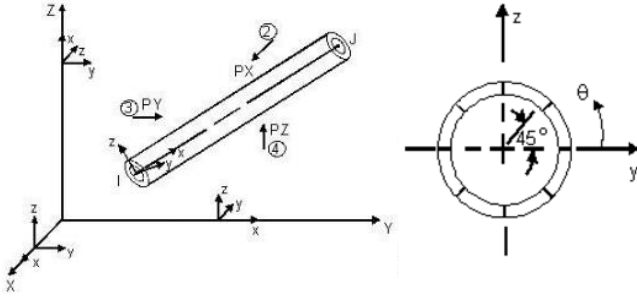


Fig. 6 The PIPE20 geometry (ANSYS 10.0 2005)

structural damage index D_s (Park and Ang 1985, Du *et al.* 2007) shown in Eq. (1), was obtained to distinguish the influence of near-fault and far-fault seismic waves on the dynamic response of single-layer reticulated shells to evaluate their structural damage.

The pipe20 element (ANSYS 10.0 2005) is a uniaxial element with tension-compression, bending, and torsion capabilities as shown in Fig. 6. The element has six degrees of freedom at each node: translations in the nodal, x , y , and z directions, and rotations about the nodal x , y , and z axes. The element has plastic, creep and swelling capabilities, and it can output nodal displacements, member forces for nodes, axial stress, maximum bending stress at the outer surface, shear strains, strain energy, and so on. In addition, there were eight integration points distributing uniformly around the cross-section of the pipe20, which can output all the data mentioned above.

4. Seismic damage evaluation of the dome

In this paper, a classic damage index, the Park-Ang index as shown in Eq. (1) (Du *et al.* 2007, Park and Ang 1985), is introduced to evaluate structural damage in single-layer reticulated shells under earthquake ground motions.

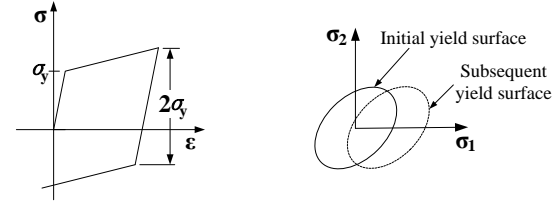
$$D_s = \frac{d_M}{d_U} + \frac{\beta}{Q_y d_U} \int dE_p \quad (1)$$

where d_M , d_U are the maximum deflection experienced by the single-layer reticulated shell during a seismic event and the ultimate deformation capacity of the same component respectively. Q_y is the yield capacity and dE_p is the dissipated energy increment. β is a constant which emphasizes the strength deterioration per cycle, where β is equal to 1.0 for general structures. Here, the dissipated energy adopted by Ansys software is

$$\int dE_p = \int \sigma_p v d\epsilon_p \quad (2)$$

It should be noted that the element volumes are constant values during a seismic event.

Additionally, the von Mises yield criterion (ANSYS 10.0 2005) as given by Eq. (3) was used to distinguish the elastic and plastic stages of the material, the material flow rule which determines the direction of plastic straining is given in Eq. (4), the stress-strain behavior of the plasticity option is a Bilinear Kinematic model and the hardening rule is a Kinematic Hardening model as shown in Fig. 7.



(a) Bilinear Kinematic

(b) Kinematic Hardening

Fig. 7 the Bilinear Kinematic and Kinematic Hardening models of the selected material

$$\sigma_e = \sqrt{\frac{1}{2}[(\sigma_1 - \sigma_2)^2 + (\sigma_2 - \sigma_3)^2 + (\sigma_3 - \sigma_1)^2]} \quad (3)$$

where σ_1 , σ_2 and σ_3 are the 1st, 2nd and 3rd principal stress respectively.

$$d\epsilon^p = \lambda \frac{\partial Q}{\partial \sigma} \quad (4)$$

where λ is a plastic multiplier, Q is the function of stress termed the plastic potential which determines the direction of plastic straining.

5. Seismic responses and damage of domes under near-fault and far-fault seismic waves

The nonlinear time-history response analysis was carried out using the finite-element package ANSYS (ANSYS 10.0 2005) on the single-layer reticulated shells with different configurations listed in Table 2 subjected to near-fault and far-fault ground motions listed in Table 1. The seismic damage of the single-layer reticulated shells was evaluated by Eq. (1) based on the nonlinear numerical analysis results.

5.1 Nonlinear dynamic response analysis

Two sets of analyses, namely the near-fault case and far-fault case, were carried out to study the influence of near-fault and far-fault seismic waves on the dynamic response of single-layer reticulated shells. Each set contains twelve as-recorded ground motion records. Fig. 8 presents the time histories of horizontal and vertical nodal displacements from nonlinear numerical analyses for near-fault and far-fault seismic waves corresponding to Table 1. It can be seen from Fig. 8 that the nonlinear dynamic response acquired from near-fault seismic waves has a considerably different displacement history than those acquired from far-fault seismic waves. In most cases, the maximum nodal displacements for near-fault seismic waves are larger than those for far-fault seismic waves although the PGA of near-fault and far-fault waves are the same, and the maximum nodal displacement values which are the same as the total nodal displacement dU are shown in Table 3.

Statistically, the mean value of the maximum nodal displacement from near-fault seismic waves is about 0.0379 m, which is 1.66 times, larger than 0.02283 m from far-fault ground motions for horizontal seismic waves. For vertical seismic waves, the mean values of the maximum nodal

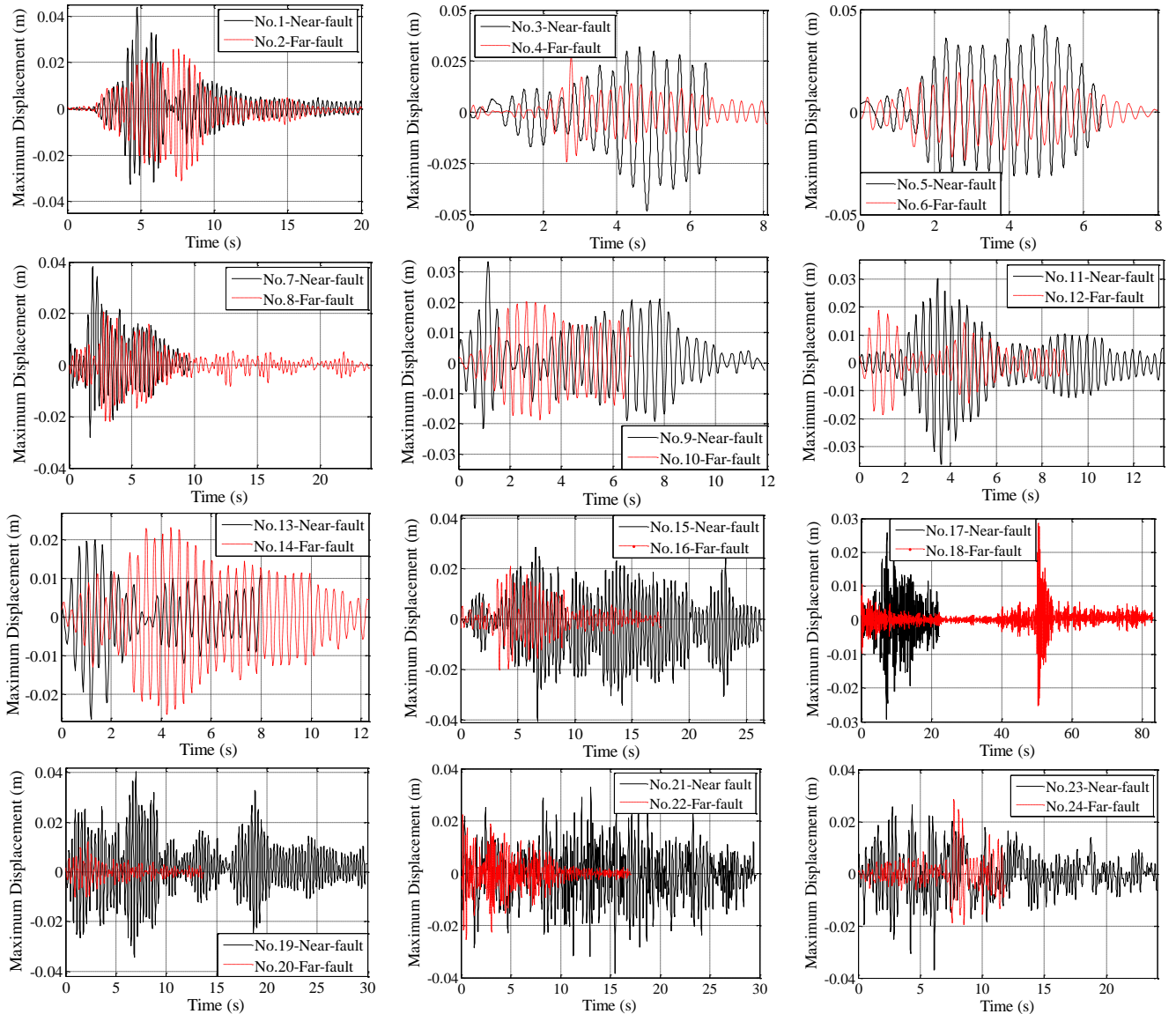


Fig. 8 The time histories of maximum horizontal displacements of Dome D40207 subject to near-fault and far-fault seismic waves from the earthquakes listed in Table 1

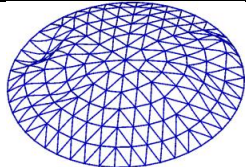
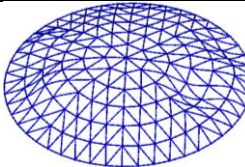
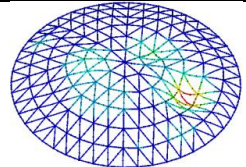
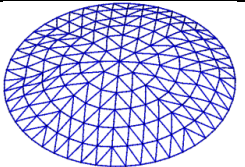
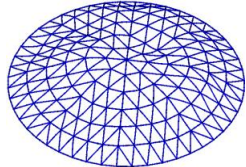
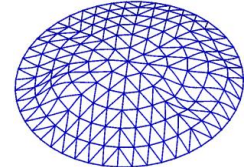
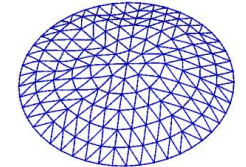
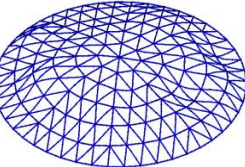
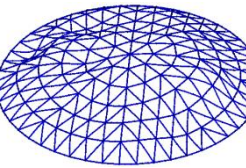
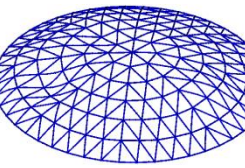
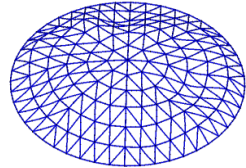
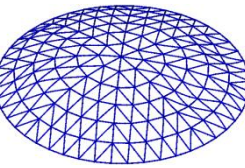
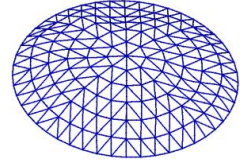
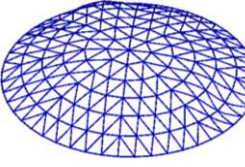
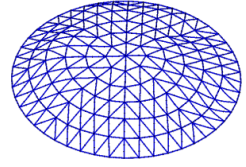
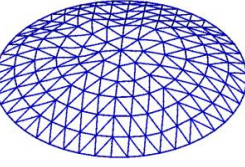
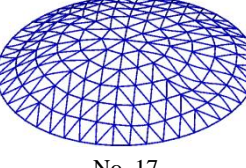
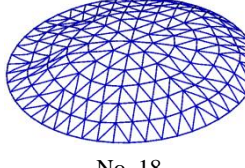
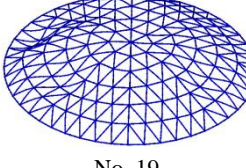
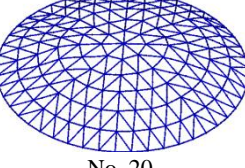




displacement from near-fault ground motions is about 0.0376 m, which is 1.41 times, larger than 0.0267 m from far-fault ground motions. The results of the numerical analysis are in accord with that of theoretical analysis of acceleration-deformation spectrum of near-fault and far fault ground motions in Fig. 3. It can also be seen from Fig. 8 that the duration of the ground motion has little effect on the nodal displacement for all those cases.

The maximum deformation of dome D40207 came from the nonlinear numerical analyses for near-fault and far-fault seismic waves are given in Table. 3. It could be found from these figures that the maximum deformation of the dome under near-fault seismic waves are significantly larger than those subjected to far-fault seismic waves for most cases, only a few of them are very closed to each other. In addition, the large deformation mainly occurs in the lower part of the dome for all ground motions.

Based on the deformation of dome D40207 shown in Table 3, the structural global strain energy obtained from

the nonlinear analysis is presented in Fig. 9 for both near-fault and far-fault seismic waves. It could be found from Fig. 9 that the global structural strain energy from near-fault seismic waves is considerably larger than those from far-fault seismic waves for most cases, only a few of them are very closed to each other. Also, for most cases, the plastic strain energy from near-fault seismic waves is larger than the values obtained from far-fault seismic waves. The maximum plastic strain energy difference is about 49 kJ for horizontal seismic waves, which is nearly 18 times the value obtained for near-fault and far-fault seismic waves at Sylmar, CA-Jensen Filtration Plant # 655 station (No.3-Near-fault) and Warm Springs # 24272 station (No.4-Far-fault) in the Northridge earthquake. For vertical seismic waves, the maximum plastic strain energy difference is about 6.53kJ, which is nearly 164 times the value obtained for near-fault and far-fault ground motions at CWB station TCU075 (No.21-Near-fault) and CWB station TCU088 (No.22-Far-fault) in Chi-Chi earthquake.

Table 3 Comparison of the maximum deformation of the dome under near-fault and far-fault seismic waves (Scale factor: 20)

Near-fault seismic wave	Far-fault seismic wave	Near-fault seismic wave	Far-fault seismic wave
			
No. 1	No. 2	No. 3	No. 4
			
No. 5	No. 6	No. 7	No. 8
			
No. 9	No. 10	No. 11	No. 12
			
No. 13	No. 14	No. 15	No. 16
			
No. 17	No. 18	No. 19	No. 20
			
No. 21	No. 22	No. 23	No. 24

Statistically, the mean values of structural total plastic strain energy from near-fault ground motions is about 18 kJ, which is nearly 4 times, larger than that from far-fault ground motions for horizontal seismic waves. For vertical seismic waves, the mean values of structural total plastic strain energy from near-fault ground motions is about 3.7 kJ, which is nearly 10 times, larger than that from far-fault seismic waves.

Generally, the dynamic responses, such as the maximum nodal displacements, structural global deformation and structural global strain energy, of dome D40207 under near-fault seismic waves are more than those obtained from far-fault seismic waves, only a few of them are very closed to each other. In addition, the seismic wave duration has little effect on the dynamic responses as shown in Fig. 8 and Fig. 9 because the selected seismic waves in Table 1 have the same peak ground acceleration but over a different duration.

5.2 Seismic damage evaluation

The seismic damage values D_s of the dome D40207 under the near-fault and far-fault seismic waves with a PGA of 1g based on Eq. (1) are listed in Table 4. Simultaneously, Table 4 also lists the frequency, the ultimate deformation capacity d_U under static load, the maximum global displacement d_M and the dissipated energy increment $\int dEp$ of dome D40207 under seismic earthquakes.

It can be seen clearly from Table 4 that the values of d_M and $\int dEp$ from near-fault seismic waves are larger than those from far-fault seismic waves for each group. Accordingly, the D_s of dome D40207 under near-fault seismic waves are more than those under far-fault seismic waves for each group, while only a few of the values are very closed to each other. The maximum difference is 0.5380 for horizontal seismic waves recorded at Sylmar and Warm Springs stations in the Northridge earthquake, and it is 0.0475 for vertical seismic waves recorded at CWB station TCU075 and CWB station TCU088 in Chi-Chi earthquake. The average value of the differences is 0.1723

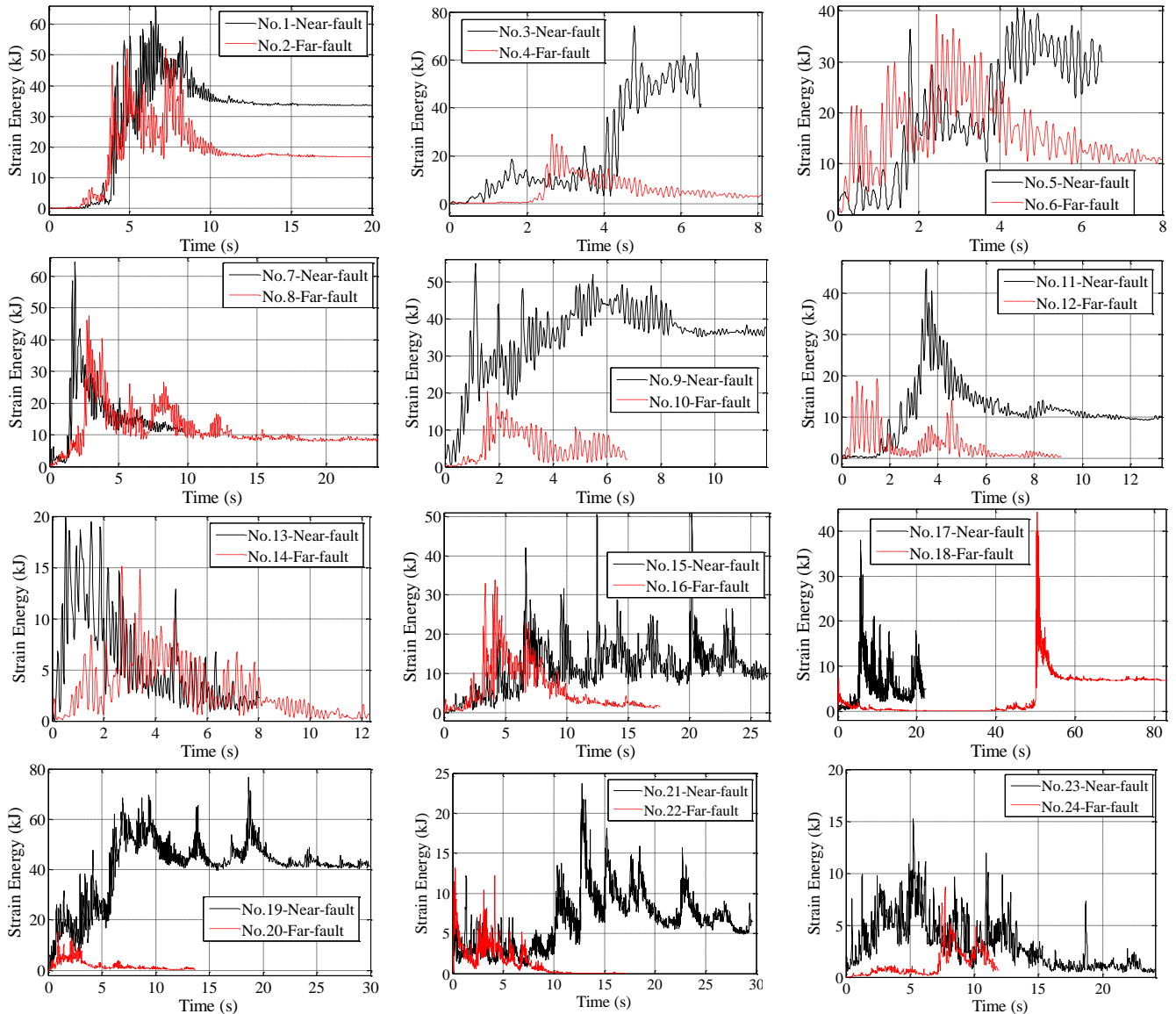


Fig. 9 The time histories of structural global strain energy of Dome D40207 under near-fault and far-fault seismic waves from the earthquakes listed in Table 1

for horizontal seismic waves, and it is 0.0614 for vertical seismic waves.

In addition, it can also be clearly seen that the duration of the seismic wave has little effect on the structural damage. This is shown in Table 4, considering the fourth group whose earthquake numbers are 7 and 8 for instance, the duration from near-fault ground motion is only 9.64s far less than 23.82s from far-ground motion, but the structural damage index is 0.621 for the near-fault seismic wave larger than 0.4229 for the far-fault seismic wave.

Lastly, the predominant frequencies of the seismic waves have a considerable effect on the structural response and damage, the closer the structural fundamental frequency and the predominant frequencies of the seismic wave, the larger the displacement, dissipated energy increment and structural damage as shown in Table 4.

To further validate the conclusions obtained from the above analysis, the nonlinear time-history response analysis was carried out using the finite-element package ANSYS

(ANSYS 10.0 2005) on the domes with different configurations listed in Table 2 subjected to near-fault seismic wave recorded at Newhall station for the Northridge earthquake, and the results are listed in Table 5.

It can also be seen from Table 5 that the values of dM , $f dE_p$ and D_s from near-fault seismic waves are relatively large. It can also further validate the fact that the closer the structural fundamental frequency and the predominant frequencies of the seismic waves are, the larger the displacements, dissipated energy increment and structural damage.

6. Conclusions

The dynamic response and seismic damage of single-layer reticulated shells subjected to near-fault and far-fault seismic waves were investigated in this paper. Nine single-layer reticulated shells were chosen for analysis, twenty-

Table 4 The seismic damage for dome D40207 under near-fault and far-fault seismic waves

Dome	Frequency	Ground motions	Duration (s)	Frequencies	Earthquake No.	d_U (m)	Q_y (N/m ²)	d_M (m)	$\int dE_p$ (kJ)	D_s
D40207	2.79	Near -fault	20.000	1.416	1	0.198	2.35×10^8	0.1092	33.62	0.5522
		Far-fault	20.000	4.736	2			0.1090	16.86	0.5509
		Near -fault	6.515	2.832	3			0.1650	52.71	0.8345
		Far-fault	8.100	4.980	4			0.0587	3.16	0.2965
		Near -fault	6.515	0.391	5			0.1050	30.08	0.5309
		Far-fault	7.980	3.711	6			0.0987	10.72	0.4987
		Near -fault	9.640	0.293	7			0.1229	11.65	0.6210
		Far -fault	23.820	2.417	8			0.0837	8.59	0.4229
		Near -fault	11.900	3.125	9			0.1140	36.30	0.5765
		Far -fault	6.700	6.641	10			0.0696	3.54	0.3516
		Near -fault	13.260	0.586	11			0.0905	9.48	0.4573
		Far -fault	9.100	2.148	12			0.0557	0.76	0.2813
		Near -fault	8.000	1.367	13			0.0657	2.87	0.3319
		Far -fault	12.280	1.514	14			0.0623	0.39	0.3147
		Near -fault	26.320	1.367	15			0.1006	10.70	0.5083
		Far -fault	17.500	1.709	16			0.0734	1.51	0.3707
		Near -fault	22.000	1.465	17			0.0872	3.57	0.4405
		Far -fault	83.040	4.150	18			0.0659	6.96	0.3330
		Near -fault	29.840	2.954	19			0.1006	42.17	0.5090
		Far -fault	13.625	4.590	20			0.0434	0.62	0.2192
		Near -fault	29.57	0.305	21			0.0404	6.57	0.2040
		Far -fault	16.98	9.448	22			0.0255	0.04	0.1288
		Near -fault	24.04	0.208	23			0.0396	0.78	0.2000
		Far -fault	11.80	0.793	24			0.0302	0.69	0.1525

Table 5 The seismic damage values of domes with different configurations subjected to near-fault seismic wave recorded at Newhall station in Northridge earthquake

Dome	The predominant frequencies (Hz)	Earthquake	First order frequencies (Hz)	d_U (m)	Q_y (N/m ²)	d_M (m)	$\int dE_p$ (kJ)	D_s
D40203	3.30	Newhall, CA-Los Angeles County Fire #24279	1.416	0.099	2.35×10^8	0.0868	845.64	0.9131
D40205	3.62			0.146		0.0764	83.19	0.5257
D40207	2.79			0.198		0.1092	33.62	0.5522
D50063	4.43			0.120		0.0468	72.37	0.3926
D50065	4.80			0.140		0.0398	0.04	0.2843
D50067	3.61			0.178		0.0509	0.05	0.2860
D60063	4.02			0.164		0.0625	411.01	0.3918
D60065	4.20			0.169		0.0568	0.30	0.3361
D60067	3.10			0.247		0.0729	0.35	0.2951

four as-recorded near-fault and far-fault strong ground motion records considered in this study were used as seismic excitations. Nonlinear seismic analyses of single-layer reticulated shells under earthquake conditions were performed considering geometric nonlinearity and material nonlinearity.

The results show that the dynamic response and seismic damage, such as larger displacements, dissipated energy increments and structural damage, of the single-layer reticulated shells under near-fault seismic waves are significantly greater than those subjected to far-fault seismic waves for most cases, only a few of them are very closed to each other. Additionally, the results also show that the closeness of the frequencies between the structures and the ground motions have a significant influence on the

dynamic response of the single-layer reticulated shells, the duration of the ground motions has little effect.

Admittedly, this paper only qualitatively evaluated the seismic effect of near-fault ground motions on the spatial structures compared to those subjected to far-fault seismic waves by nonlinear numerical analysis. In future research, the sample size of the ground motions will be increased and carry out more systematic research for the spatial structures, obtain some quantitative conclusions serving structural design.

Acknowledgements

The present work has been conducted with the financial

support from the National Natural Science Foundation of China (Grant No. 51608452). The authors also thank the financial support from the Chinese Universities Scientific Fund under Grant Nos. 2682015CX009EM, RC2015-02. Special thanks to all the staffs in Space Structure Research Center of Harbin Institute of Technology for their valuable suggestions and help. In addition, the authors thank the anonymous reviewers and the Editors for their constructive comments and advice that helped greatly in improving the quality of this manuscript.

References

- Alonso-Rodriguez, A. and Miranda, E. (2015), "Assessment of building behavior under near-fault pulse-like ground motions through simplified models", *Soil. Dyn. Earthq. Eng.*, **79**(Part A), 47-58.
- ANSYS 10.0 (2005), Theory reference, ANSYS Inc.
- Ba, P.F., Zhang, Y.G., Wu, J.Z. and Zhang, Z.H. (2015), "The failure criterion of single-layer spherical lattice shell based on kinetic energy", *Math. Probl. Eng.*, **2015**, Article ID 485710, 7.
- Bai, Y., Gong, L.F. and Yang, Y. (2015), "Elasto-plastic bearing capacity of four types of single-layer reticulated shell structures under fire hazards", *Int. J. Struct. Stab. Dy.*, **15**, 1450051-1-15.
- Brandes, K. and Vogel, A. (1998), *Mitigating the Impact of Impending Earthquakes: Earthquake Prognostics Strategy Transferred into Practice*, CRC Press, Boca Raton, State of Florida, USA.
- Bruno, L., Sassone, M. and Fiammetta, V. (2016), "Effects of the equivalent geometric nodal imperfections on the stability of single layer grid shells", *Eng. Struct.*, **112**, 184-199.
- Cao, Y.N., Meza-Fajardo, K.C., Mavroeidis, G.P. and Papageorgiou, A.S. (2016), "Effects of wave passage on torsional response of symmetric buildings subjected to near-fault pulse-like ground motions", *Soil. Dyn. Earthq. Eng.*, **88**, 109-123.
- COSMOS Virtual Data Center, <http://db.cosmos-eq.org/scripts/default.plx>
- CPA (2011), *Seismic design Code and Commentary for Building*, Construction and Planning Agency, Ministry of Interior Affairs, Taipei, Taiwan. (in Chinese)
- Du, W.F., Gao, B.Q. and Dong, S.L. (2007), "Double-control criterion of dynamical strength failure for single-layer latticed shells", *J. Zhejiang Univ. Eng. Sci.*, **41**(11), 1916-1920. (in China)
- Enderami, S.A., Beheshti-Aval, S.B. and Saadeghvaziri, M.A. (2014), "New energy based approach to predict seismic demands of steel moment resisting frames subjected to near-fault ground motions", *Eng. Struct.*, **72**, 182-192.
- Fabio, M. and Mirko, M. (2016), "Nonlinear seismic analysis of irregular r.c. framed buildings base-isolated with friction pendulum system under near-fault excitations", *Soil. Dyn. Earthq. Eng.*, **90**, 299-312.
- Fan, F., Cao, Z.G. and Shen, S.Z. (2010), "Elasto-plastic stability of single-layer reticulated shells", *Thin Wall Struct.*, **48**, 827-836.
- Fan, F., Li, Y.G., Zhi, X.D. and Li, L. (2014), "Comparison of seismic response of single-layer reticulated dome under uniform and incoherence three-directional excitations", *Int. J. Steel Struct.*, **14**(4), 855-863.
- GB 50011-2010 (2010), *Code for Seismic Design of Building*, China Architecture & Building Press, Beijing, China. (in Chinese)
- Hall, J.F., Heaton, T.H., Halling M.W. and Wald, D.J. (1995), "Near-source ground motion and its effects on flexible buildings", *Earthq. Spectra*, **11**(4), 569-605.
- Housner, G.W. and Hudson, D.E. (1958), "The port huene earthquake of march 18, 1957", *Bull. Seismol. Soc. Am.*, **48**, 163-168.
- IBC-2012 (2011), 2012 International Building Code, International Code Council, Inc, USA.
- Kalkan, E. and Kunnath, S.K. (2006), "Effects of fling step and forward directivity on seismic response of buildings", *Earthq. Spectra*, **22**(2), 367-390.
- Kaoru, Y., Kohei, F. and Izuru, T. (2011), "Instantaneous earthquake input energy and sensitivity in base-isolated building", *Struct. Des. Tall. Spec.*, **20**(6), 631-648.
- Kong, D.W., Fan, F. and Zhi, X.D. (2014), "Seismic performance of single-layer lattice shells with VF-FPB", *Int. J. Steel Struct.*, **14**, 901-911.
- Kotaro, K. and Izuru, T. (2015), "Critical earthquake response of elastic-plastic structures under near-fault ground motions (Part 2: Forward-directivity input)", *Front. Built Environ.*, **1**, 1-11.
- Li, Y.G., Fan, F. and Hong, H.P. (2014), "Effect of support flexibility on seismic responses of a reticulated dome under spatially correlated and coherent excitations", *Thin Wall Struct.*, **82**, 343-351.
- Liu C.G. and Li, H.J. (2010), "A novel method to calculate the dynamic reliability of space structures subjected to multi-dimensional multi-support excitations", *Int. J. Space Struct.*, **25**, 25-34.
- Liu, W.Z. and Ye, J.H. (2014), "Collapse optimization for domes under earthquake using a genetic simulated annealing algorithm", *J. Constr. Steel. Res.*, **97**, 59-68.
- Ma, H.H., Fan, F., Wen, P., Zhang, H. and Shen, S.Z. (2015), "Experimental and numerical studies on a single-layer cylindrical reticulated shell with semi-rigid joints", *Thin Wall Struct.*, **86**, 1-9.
- Ma, H.H., Fan, F., Zhong, Z. and Cao, Z.G. (2013), "Stability analysis of single-layer elliptical parabolic latticed shells with semi-rigid joints", *Thin Wall Struct.*, **72**, 128-138.
- Ma, J.L., Fan, F., Wu, C.Q. and Zhi, X.D. (2015), "Counter-intuitive collapse of single-layer reticulated domes subject to interior blast loading", *Thin Wall Struct.*, **96**, 130-138.
- Ma, J.L., Wu, C.Q., Zhi, X.D. and Fan, F. (2014), "Prediction of confined blast loading in single-layer lattice shells", *Adv. Struct. Eng.*, **17**, 1029-1043.
- Malhotra, P.K. (1999), "Response of buildings to near-field pulse-like ground motions", *Earthq. Eng. Struct. Dyn.*, **28**(11), 1309-1326.
- Masaeli, H., Khoshnoudian, F. and Hadikhan Tehrani, M. (2014), "Rocking isolation of nonductile moderately tall buildings subjected to bidirectional near-fault ground motions", *Eng. Struct.*, **80**, 298-315.
- Mavroeidis, G.P., Dong, G. and Papageorgiou, A.S. (2004), "Near-fault ground motions, and the response of elastic and inelastic single-degree-of-freedom (SDOF) systems", *Earthq. Eng. Struct. Dyn.*, **33**, 1023-1049.
- Minasidis, G., Hatzigeorgiou, G.D. and Beskos, D.E. (2014), "SSI in steel frames subjected to near-fault earthquakes", *Soil. Dyn. Earthq. Eng.*, **66**, 56-68.
- Nie, G.B., Zhi, X.D., Fan, F. and Dai, J.W. (2014), "Seismic performance evaluation of single-layer reticulated dome and its fragility analysis", *J. Constr. Steel. Res.*, **100**, 176-182.
- Park, Y.J. and Ang, A.H.S. (1985), "Mechanistic seismic damage model for reinforced concrete", *J. Struct. Eng.*, **111**(4), 722-739.
- Ramalingam, R. and Jayachandran, S.A. (2015), "Postbuckling behavior of flexibly connected single layer steel domes", *J. Constr. Steel. Res.*, **114**, 136-145.
- Rodriguez-Marek, A. and Cofer, W. (2007), "Dynamic response of bridges to near-fault, forward directivity ground motions", Report No. WA-RD 689.1, Civil and Environmental

- Engineering Department, Washington State University, Washington, USA.
- Ueno, K., Takewaki, I. and Moustafa, A. (2010), "Critical earthquake loads for SDOF inelastic structures considering evolution of seismic waves" *Eng. Struct.*, **12**, 147-162.
- Wang, G.H., Zhang, S.R., Wang, C. and Yu, M. (2014), "Seismic performance evaluation of dam-reservoir-foundation systems to near-fault ground motions", *Nat. Hazard.*, **72**(2), 651-674.
- Wu, G., Zhai, C.H., Li, S. and Xie, L.L. (2014), "Effects of near-fault ground motions and equivalent pulses on Large Crossing Transmission Tower-line System", *Eng. Struct.*, **77**, 161-169.
- Yan, J.C., Qin, F., Cao, Z.G., Fan, F. and Mo, Y.L. (2016), "Mechanism of coupled instability of single-layer reticulated domes", *Eng. Struct.*, **114**, 158-170.
- Yan, R.Z., Chen, Z.H., Wang, X.D., Xiao, X. and Yang, Y. (2014), "Calculation theory and experimental study of the K6 single-layer reticulated shell", *Int. J. Steel Struct.*, **14**(2), 195-212.
- Yang, S., Mavroeidis, G.P., Ucak, A. and Tsopelas, P. (2017), "Effect of ground motion filtering on the dynamic response of a seismically isolated bridge with and without fault crossing considerations", *Soil. Dyn. Earthq. Eng.*, **92**, 183-191.
- Ye, J.H., Zhang, Z.Q. and Chu, Y. (2011), "Strength behavior and collapse of spatial-reticulated structures under multi-support excitation", *Sci. China Technol. Sci.*, **54**, 1624-1638.
- Ye, J.H., Zhang, Z.Q. and Chu, Y. (2011), "Strength failure of spatial reticulated structures under multi-support excitation", *Earthq. Eng. Vib.*, **10**(1), 21-36.
- Yu, Z.W., Zhi, X.D., Fan, F. and Chen, L. (2011), "Effect of substructures upon failure behavior of steel reticulated domes subjected to the severe earthquake", *Thin Wall Struct.*, **49**, 1160-1170.
- Zhai, X.M. and Wang, Y.H. (2013), "Modeling and dynamic response of steel reticulated shell under blast loading", *Shock Vib.*, **20**, 19-28.
- Zhai, X.M., Wang, Y.H. and Huang, M. (2013), "Performance and protection approach of single-layer reticulated dome subjected to blast loading", *Thin Wall Struct.*, **73**, 57-67.
- Zhang, S.R. and Wang, G.H. (2013), "Effects of near-fault and far-fault ground motions on nonlinear dynamic response and seismic damage of concrete gravity dams", *Soil. Dyn. Earthq. Eng.*, **53**, 217-229.
- Zhi, X. D., Feng, F. and Shen, S. Z. (2007), "Failure mechanisms of single-layer reticulated domes subjected to earthquakes", *J. IAASS.*, **48**(1): 29-44.
- Zhong, J., Zhi, X. D. and Fan, F. (2016), "A dominant vibration mode-based scalar ground motion intensity measure for single-layer reticulated domes", *Earthq. Struct.*, **11**(2), 245-264.
- Zhu, N.H. and Ye, J.H. (2014), "Structural vulnerability of a single-layer dome based on its form", *J. Eng. Mech.*, **140**(1), 112-127.